catalysts

MDPI

Article

Effects of Alkali Metals on Nickel/Alumina Catalyzed Ethanol Dry Reforming

Se-Won Park †, Dongseok Lee †, Seung-Ik Kim, Young Jin Kim, Ji Hoon Park, Iljeong Heo, Tae Sun Chang * and Jin Hee Lee *

Center for Environment and Sustainable Resources, Korea Research Institute of Chemical Technology, Daejeon 34114, Korea; parksw@krict.re.kr (S.-W.P.); lds0428@krict.re.kr (D.L.); sikim@krict.re.kr (S.-I.K.); yjkim03@krict.re.kr (Y.J.K.); jihpark@krict.re.kr (J.H.P.); zaiseok@krict.re.kr (I.H.)

* Correspondence: tschang@krict.re.kr (T.S.C.); leejh@krict.re.kr (J.H.L.); Tel.: +82-42-860-7598 (J.H.L.); Fax: +82-42-860-7593 (J.H.L.)

† Se-Won Park and Dongseok Lee contributed equally to this work.

Abstract: Although ethanol dry reforming is an attractive carbon utilization technology, problems of severe coke formation and low catalytic activity should be solved for realization of the technology. We demonstrate the effects of alkali metal additives (lithium, sodium, and potassium) on nickel catalyzed ethanol dry reforming. Potassium doped nickel catalyst (Ni/K_2O-Al_2O_3) showed enhanced catalytic activity and durability in ethanol dry reforming. Thermogravimetric analysis (TGA) showed that Ni/K_2O-Al_2O_3 had a high resistance to coke formation. The amounts of coke formed on Ni/K_2O-Al_2O_3 were 1/3 lower than the amounts of coke formed on Ni/Al_2O_3. The total coke quantities were closely correlated to the number of basic sites of the nickel catalysts. Raman spectroscopy and transmission electron microscopy analyses revealed that the alkali metals control the coke formation on the catalysts.

Keywords: carbon capture and utilization; ethanol dry reforming; alkali metal; nickel catalyst

check for updates

Citation: Park, S.-W.; Lee, D.; Kim, S.-I.; Kim, Y.J.; Park, J.H.; Heo, I.; Chang, T.S.; Lee, J.H. Effects of Alkali Metals on Nickel/Alumina Catalyzed Ethanol Dry Reforming. *Catalysts* **2021**, *11*, 260. https://doi.org/10.3390/catal11020260

Academic Editor: Leonarda Francesca Liotta

Received: 12 January 2021

Accepted: 12 February 2021

Published: 15 February 2021

Publisher's Note: MDPI stays neutral with regard to jurisdictional claims in published maps and institutional affiliations.

Copyright: © 2021 by the authors. Licensee MDPI, Basel, Switzerland. This article is an open access article distributed under the terms and conditions of the Creative Commons Attribution (CC BY) license (https://creativecommons.org/licenses/by/4.0/).

1. Introduction

Greenhouse gases (GHGs) have been cited as a main cause of global warming. Carbon dioxide especially is the main GHG, accounting for 88% of global warming [1–4]. Carbon capture and utilization (CCU) is of enormous interest to mitigate global warming [5,6]. As one type of CCU technology, methane dry reforming has been widely studied due to its high carbon dioxide conversion and production of a useful gas mixture, synthesis gas (Equation (1)). Synthesis gas is a key substance that can be converted into a number of platform chemicals such as methanol, dimethyl ether, olefins, synthetic fuel, and ammonia.

$$CH_4 + CO_2 \rightarrow 2CO + 2H_2 \ (\triangle H_{298K} = +247 \text{ kJ mol}^{-1}) \quad (1)$$

Although methane dry reforming is a valuable CCU technology, it is necessary to replace petroleum-derived methane with non-petroleum derived chemicals for effective carbon reduction and termination of additional carbon emission. The utilization of alternative carbon sources derived from waste plastic, biomass and/or sewage sludge is an attractive challenge. The thermal decomposition of alternative carbon sources produces useful chemicals including ethanol, acetic acid, ethylene glycol, propionic acid, phenol, etc. [7]. In this study, for CCU, we take advantage of ethanol, which is obtained by thermal decomposition of numerous types of biomass, and is highly stable at ambient conditions, non-toxic, and readily stored and transported [8–10].

One ethanol molecule reacts with one carbon dioxide molecule to produce a one to one ratio of carbon monoxide and hydrogen, similar to methane dry reforming (Equation (2)). For ethanol dry reforming, nickel catalysts have most widely been studied. A number

of transition metal catalysts were used for reforming reactions. Among these catalysts, compared to novel metal catalysts, the nickel based catalysts have been commercialized and the most widely used due to high catalyst activity, a low price, and favorable C-C bond-breaking capability [11,12]. However, existing nickel-based catalysts have some problems such as carbon deposition, sintering, sulfur poisoning, and the formation of toxic nickel compound [13]. For example, Assaf and co-workers [14] reported nickel supported on Y_2O_3-ZrO_2 for ethanol dry reforming and found that the oxygen vacancy in Y_2O_3-ZrO_2 strongly interacted with nickel oxide to hamper catalyst agglomeration. Hu and co-workers [11] investigated the effects of temperature and carbon dioxide/ethanol ratios on coke formation during ethanol dry reforming. Their study pointed out that high temperature and high carbon dioxide concentration are required to reduce coke formation. Vo's research group [15] reported that performance of nickel catalysts can be enhanced by promotion with cobalt and lanthanum. They also employed lanthanum promoted copper alumina catalyst for the ethanol dry reforming [16]. Cao et al., utilized reducible oxide support for ethanol dry reforming. CuCeZr showed the best activity and durability among the tested catalysts [17]. Lastly, Aziz and co-workers [18] reported that the coke could be removed by the gasification, and it could be enhanced by the basic site of the catalyst.

$$C_2H_5OH + CO_2 \rightarrow 3CO + 3H_2 \ (\triangle H_{298K} = +\ 296.7\ kJ\ mol^{-1}) \quad (2)$$

Numerous studies were conducted to improve the catalytic activity and stability. However, the coke formation mechanism is not clear and the catalyst stability is still needed to be improved. In this study, we report a coke-resistant ethanol dry reforming catalyst via the addition of alkali metals to Ni/Al_2O_3. The alkali metals successfully reduced the coke formation and consequently enhanced catalyst stability. Detailed analyses of deposited coke revealed that the basic sites of the alkali metal promoted catalytic performance and hampered the coke deposition as well. The roles of alkali metals both on suppressing coke formation and accelerating coke removal were studied.

2. Results and Discussion

2.1. Ethanol Dry Reforming Catalyzed by Ni/Al_2O_3

The catalytic activity of Ni/Al_2O_3 on ethanol dry reforming was tested under a flow of 1:1 mixture of ethanol and carbon dioxide at 700 °C (Figure 1). The initial carbon dioxide and ethanol conversion was higher; however, carbon dioxide conversion sharply decreased after 1 h and ethanol conversion decreased after 2 h. These catalytic activity decreases were closely related to product gas composition. The time on stream concentrations of desired products, carbon monoxide and hydrogen, were correspondingly decreased with ethanol and carbon dioxide conversion. Interestingly, methane and ethylene appeared until 1 h and 2 h of the reaction, respectively, and then disappeared. This might be due to the rapid alteration of catalytic active sites. Because methane and ethylene, which can be produced via ethanol dehydrogenation and dehydration, respectively (Scheme 1), are by-products of ethanol dry reforming [19,20], we can infer that ethanol dry reforming initially includes ethanol dehydrogenation and dehydration as side reactions. Ethanol and carbon dioxide conversion without nickel are shown in Figure S1. Lower carbon dioxide conversion on Al_2O_3 indicates that nickel is pivotal to activate carbon dioxide molecule.

It is well known that methane and ethylene generate coke on the catalyst surface via decomposition reaction [21]. Thus, the catalytic activity decrease observed in the initial 2 h might originate from the decomposition of methane and ethylene, and the ensuing coke formation. The simultaneous termination of intense catalyst deactivation and formation of methane and ethylene indicate that catalyst deactivation is associated with methane and ethylene. In addition, the initial coke likely formed on the catalyst active site related to the ethanol dehydrogenation and dehydration rather than the carbon dioxide activation.

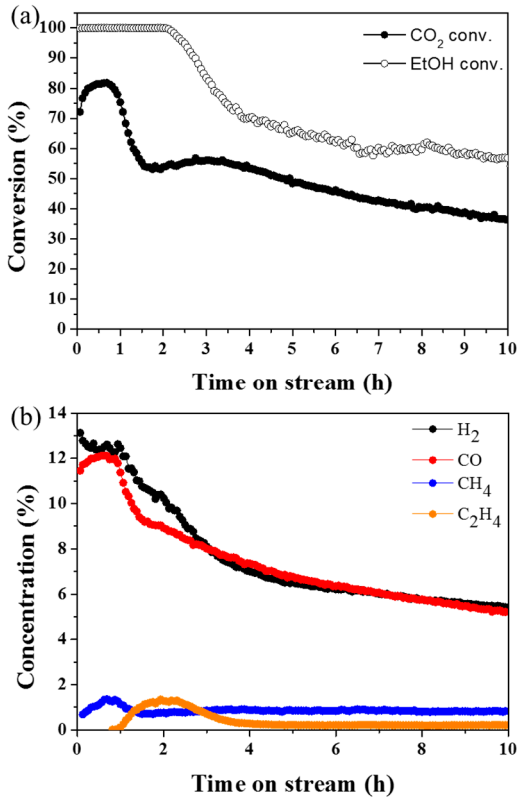


Figure 1. Plots of Ni/Al_2O_3 catalyzed ethanol dry reforming performed at 700 °C, 40,000 h^{-1} gas hourly space velocity (GHSV), and ethanol/carbon dioxide ratio of 1. (**a**) Carbon dioxide and ethanol conversion, and (**b**) product gas composition.

$$C_2H_5OH \longrightarrow H_2 + CO + CH_4 \quad \text{(dehydrogenation)}$$

$$C_2H_5OH \longrightarrow C_2H_4 + H_2O \quad \text{(dehydration)}$$

Scheme 1. Ethanol dehydrogenation and dehydration pathway.

The catalyst durability is improved by additional carbon dioxide stream. There was no critical catalyst deactivation when the carbon dioxide/ethanol ratio was 3 (Figure 2a). The monitoring of the product gases showed that the additional carbon dioxide flow inhibited the formation of methane and ethylene (Figure 2b). These results further support that the rapid catalyst deactivation and coke formation at the low ethanol to carbon dioxide ratio originates from the formation of unwanted byproducts, such as methane and ethylene. Reduction of methane and ethylene concentrations signifies that the carbon dioxide might promote the direct reaction of ethanol and carbon dioxide by preventing ethanol dehydrogenation and dehydration. In addition, carbon dioxide can hinder coke formation via reverse Boudouard reaction [22,23].

2.2. Characterizations of Alkali Metal Promoted Ni/Al_2O_3

Our initial results show that the minimization of coke formation by carbon dioxide addition is crucial for stable catalytic performance of ethanol dry reforming. We thus utilized alkali metal additives to the nickel catalyst to increase the local carbon dioxide concentration adjacent to active sites. The utilization of alkali or alkali-earth metals for carbon dioxide adsorption has widely been studied; this process exploits the high affinity of basic alkali or alkali metal sites toward carbon dioxide, which attributed to the highly oxidized and electron deficient characteristic of carbon dioxide [24–26].

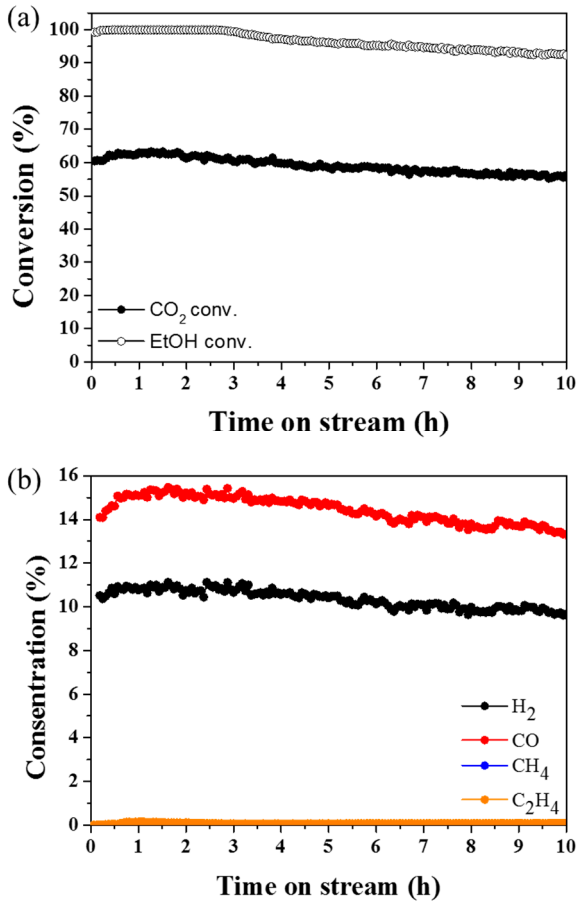


Figure 2. Plots of Ni/Al_2O_3 catalyzed ethanol dry reforming process performed at 700 °C, 40,000 h^{-1} gas hourly space velocity (GHSV), and carbon dioxide/ethanol ratio of 3. (**a**) Carbon dioxide and ethanol conversion, and (**b**) product gas composition.

The crystal structures of the prepared catalysts were determined by X-ray diffraction (XRD) analyses (Figure 3). Sodium and potassium did not alter the original structure of γ-Al_2O_3. The XRD patterns of Na_2O-Al_2O_3 and K_2O-Al_2O_3 were almost identical to that of γ-Al_2O_3 [27]. However, lithium produced lithium-aluminum mixed oxide phase. Moreover, the sharp peaks of Li_2O-Al_2O_3 signify that the crystallinity of the resulting material increased after lithium incorporation. The XRD patterns of Ni/Al_2O_3, Ni/K_2O-Al_2O_3, and Ni/Na_2O-Al_2O_3 showed no specific diffraction patterns related to nickel oxide. The absence of any diffractions corresponding to nickel oxide indicates that the impregnated nickel oxide is either well dispersed over the supports or forms a new crystal phase such as $NiAl_2O_4$ [28]. The XRD patterns of Ni/Li_2O-Al_2O_3 are almost identical to the XRD patterns of Li_2O-Al_2O_3. Nickel did not affect the crystal structure of Li_2O-Al_2O_3 and likely forms small nickel oxide nanoparticles. The existence of both small nickel oxide particles and $NiAl_2O_4$ was confirmed by H_2-temperature programmed reduction (H_2-TPR) experiments (Figure S2). The reduction peak at lower temperatures (400 °C) corresponds to the reduction of the well dispersed nickel oxide to metallic nickel and large reduction peak at high temperature (850 °C) corresponds to the reduction of $NiAl_2O_4$ [29,30].

N_2-adsorption and desorption isotherm analysis was implemented to elucidate the pore structure of the prepared catalysts. All the prepared catalysts showed type IV isotherm curves with hysteresis at $p/p_o > 0.6$. These nitrogen isotherm curves indicate that the mesoporous nature of the Al_2O_3 based materials is maintained after alkali metal and nickel incorporation (Figure S3). Brunauer–Emmett–Teller (BET) surface area and total pore volume of Li_2O-Al_2O_3 were lower than those of other M_2O-Al_2O_3 supports (Table 1, entries 1–4). The low total pore volume and large average pore size of Li_2O-Al_2O_3 compared to

other types of M_2O-Al_2O_3 indicate that the added lithium blocks small pores of γ-Al_2O_3 by formation of lithium-aluminum mixed oxide, which was observed by XRD (Figure 3). The pore structures of Na_2O-Al_2O_3 and K_2O-Al_2O_3 were not severely changed. Only slight decreases of BET surface area and pore volume were observed (Table 1, entries 3–4, and Figure S4). The nickel incorporation as well slightly reduced the BET surface area and pore volume of all M_2O-Al_2O_3 samples, but there were no significant alterations of pore structure (Table 1, entries 5–8, and Figure S4) [31]. Transmission electron microscopy (TEM) images of the reduced Ni catalysts are shown in Figure S5. At all images, nickel nanoparticles were dispersed on the Al_2O_3 support. The respective average nickel particle sizes of Ni/Al_2O_3, Ni/Li_2O-Al_2O_3, Ni/Na_2O-Al_2O_3, and Ni/K_2O-Al_2O_3 is 15.5 nm, 24.7 nm, 24.7 nm, and 32.9 nm. The added alkali metals were located near the nickel nanoparticles and these would make the particle size bigger.

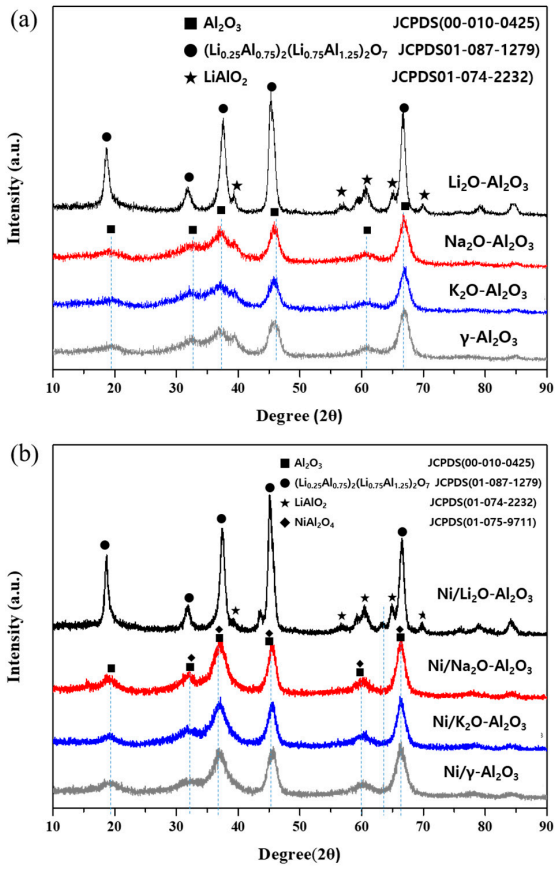


Figure 3. XRD patterns of (**a**) M_2O-Al_2O_3, and (**b**) Ni/M_2O-Al_2O_3.

2.3. Ethanol Dry Reforming Catalyzed by Alkali Metal Modified Ni/Al_2O_3

To evaluate the influences of alkali metal additives, Ni/M_2O-Al_2O_3 samples were tested for ethanol dry reforming. The reactions were performed at 700° stream conversion of ethanol and carbon dioxide. The highest carbon dioxide and ethanol conversion appeared with Ni/K_2O-Al_2O_3. Here as well, similar to the case of Ni/Al_2O_3, decreases of carbon dioxide and ethanol conversion were observed after 1 h of reaction, which means the coke forms on the catalyst surface. However, the deactivation rates after initial sharp deactivation were varied between catalysts. The catalyst deactivation rates were evaluated by calculating slopes of the time on stream carbon dioxide conversion plots (Figure 4). The slopes were calculated using carbon dioxide conversion between 2 h and 10 h. The calculated slopes of time on stream plots are as follows; −0.96 for Ni/K_2O- Al_2O_3 > −1.49 for Ni/Na_2O-Al_2O_3 > −2.77 for Ni/Al_2O_3 > −3.01 for Ni/Li_2O-Al_2O_3. Potassium and sodium containing catalysts exhibited enhanced catalyst stability than Ni/Al_2O_3. On the

other hand, the addition of lithium deteriorated the catalytic ethanol dry reforming in terms of both activity and durability. The lowest surface area and pore volume, attributed to the formation of lithium-aluminum mixed oxide, might influence the performance of the nickel catalyst. The time on stream methane and ethylene distributions were examined (Figure S6). The concentrations of methane and ethylene were increased and disappeared at the beginning of the reaction, and the concentration difference between four catalysts was lower than 0.5%. These results indicate that the rate of methane and ethylene formation is similar, but coke formation is suppressed by alkali metal sites. Catalytic activity at lower temperatures than 700 °C (550 °C, 600 °C, and 650 °C) were also evaluated (Figure S7). Obviously, $Ni/K_2O\text{-}Al_2O_3$ exhibited the better catalytic activity for both carbon dioxide and ethanol conversion than Ni/Al_2O_3, at all temperatures. In addition, alkali metal added nickel catalysts showed carbon dioxide conversion at 550 °C while the Ni/Al_2O_3 were still not activated.

Table 1. Brunauer–Emmett–Teller (BET) surface area and pore structure information of prepared catalysts analyzed by N_2-isothrem.

Entry	Sample	Surface Area (m^2/g)	Pore Size (nm)	Pore Volume (cm^3/g)
1	Al_2O_3	205	9	0.48
2	$Li_2O\text{-}Al_2O_3$	89	16	0.41
3	$Na_2O\text{-}Al_2O_3$	142	11	0.41
4	$K_2O\text{-}Al_2O_3$	166	10	0.41
5	Ni/Al_2O_3	143	11	0.4
6	$Ni/Li_2O\text{-}Al_2O_3$	65	17	0.27
7	$Ni/Na_2O\text{-}Al_2O_3$	127	9	0.3
8	$Ni/K_2O\text{-}Al_2O_3$	137	9	0.31

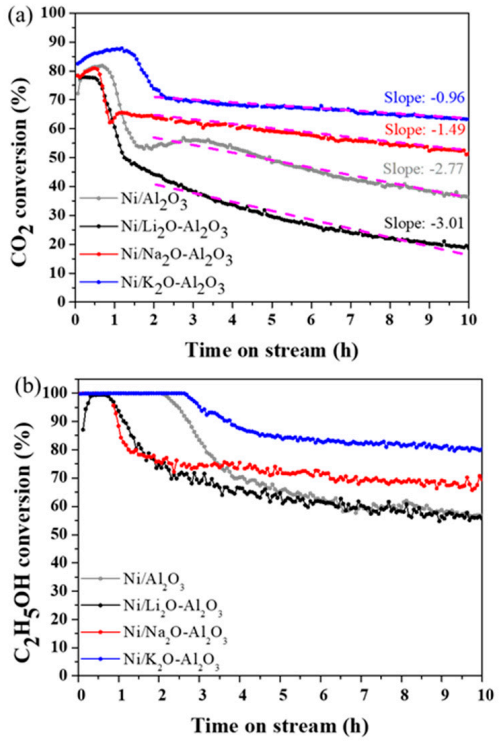


Figure 4. Plots of $Ni/M_2O\text{-}Al_2O_3$ catalyzed ethanol dry reforming performed at 700 °C, 40,000 h^{-1} GHSV, and carbon dioxide/ethanol ratio of 1. (**a**) Carbon dioxide conversion, and (**b**) ethanol conversion.

2.4. Characterizations of Deposited Coke

Since the catalytic activity and durability are closely related to the coke formation, we examined the cokes deposited on the catalysts after 10 h of ethanol dry reforming. As compared to fresh catalysts, coke formation, which caused catalytic activity decrease, was observed in TEM images of all the catalysts (Figure S5 and Figure 5). After the reforming reaction, amorphous carbon and nanotube shaped carbon were mainly observed. Energy-dispersive X-ray spectroscopy (EDS) analyses on spent catalysts showed the presence of carbon around the nickel catalysts more clearly (Figure S8).

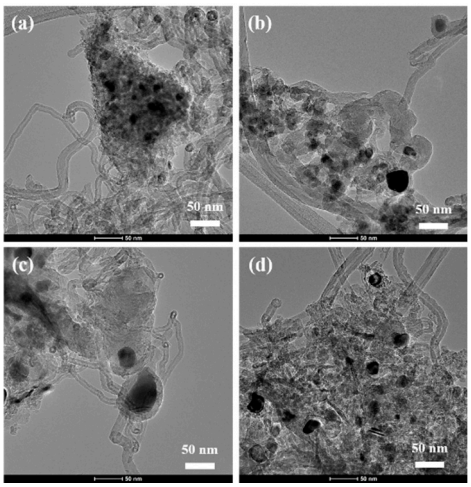


Figure 5. TEM images of spent catalysts after 10 h of ethanol dry reforming. (**a**) Ni/Al_2O_3, (**b**) Ni/Li_2O-Al_2O_3, (**c**) Ni/Na_2O-Al_2O_3, and (**d**) Ni/K_2O-Al_2O_3.

The structure of carbon was further studied by Raman spectroscopy. The D peak at around 1330 cm^{-1}, which attributes to the disordered carbon structure, and the G peak at around 1550 cm^{-1}, which attributes to the graphitic sp^2 carbon structure were observed in the Raman spectra of the four catalysts (Figure 6) [32–34]. The I_D/I_G ratios of the catalysts were 1.5, 0.98, 0.90, and 1.0 for Ni/Al_2O_3, Ni/Li_2O-Al_2O_3, Ni/Na_2-Al_2O_3, and Ni/K_2O-Al_2O_3, respectively. Since amorphous carbon constitutes more disordered structure than graphitic carbon, the I_D/I_G ratios in the Raman spectra of carbon materials increase as the amounts of amorphous carbon increases. Thus, the higher I_D/I_G ratio of Ni/Al_2O_3 signifies that the more amorphous carbon forms on Ni/Al_2O_3 than on the alkali metal promoted catalysts, and the alkali metal additives lead to the formation of different carbon structure.

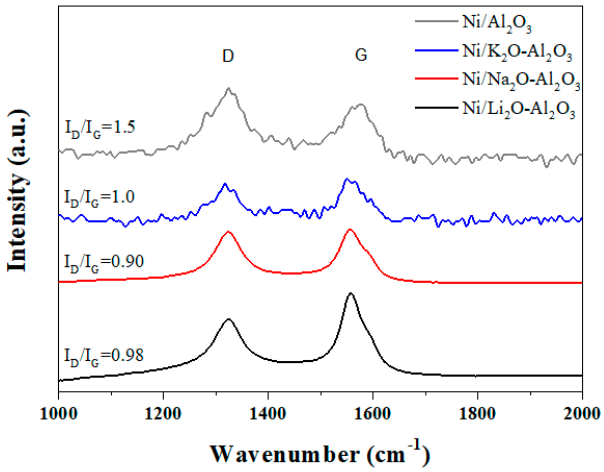


Figure 6. Raman spectra of catalysts after 10 h of ethanol dry reforming.

Since the amounts of deposited coke were also examined by TGA (Figure 7), the weight loss, which is related to the oxidation of carbon species, mainly started after 370 °C. The beginning temperature of coke removal of Ni/Al_2O_3 was 460 °C, which is about 100 °C higher than that of other catalysts. The lower coke removal initiation temperature of alkali metal promoted catalysts indicates that the alkali metals oxidize the carbon more easily than Ni/Al_2O_3. As well as the coke oxidation rate, the total coke amounts are also controlled by alkali metal additives. The alkali metal promoted catalysts showed much smaller amounts of coke formation (Figure 7). The suppression of coke formation by alkali metal additives is more pronounced in the amounts of coke relative to the amounts of reacted ethanol (Figure 8). In general, the amounts of coke deposition increase as conversion increases. It is therefore more reasonable to compare the amounts of deposited coke relative to conversion of coke generation source, namely ethanol in this case. Figure 8 shows that all the alkali metal additives successfully control coke deposition. The amount of coke relative to converted ethanol catalyzed by $Ni/K_2O\text{-}Al_2O_3$ is one-third that of Ni/Al_2O_3. These results show that not only the inhibition of coke formation but also the selective conversion of ethanol and carbon dioxide to synthesis gas are accomplished by alkali metal additives.

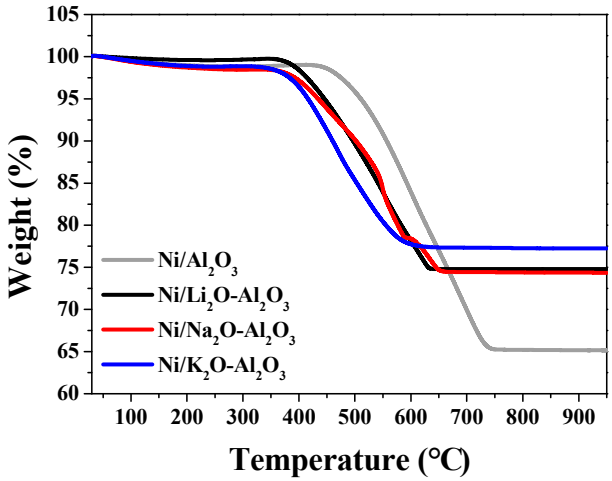


Figure 7. Thermogravimetric analysis (TGA) curves of catalysts after 10 h of ethanol dry reforming.

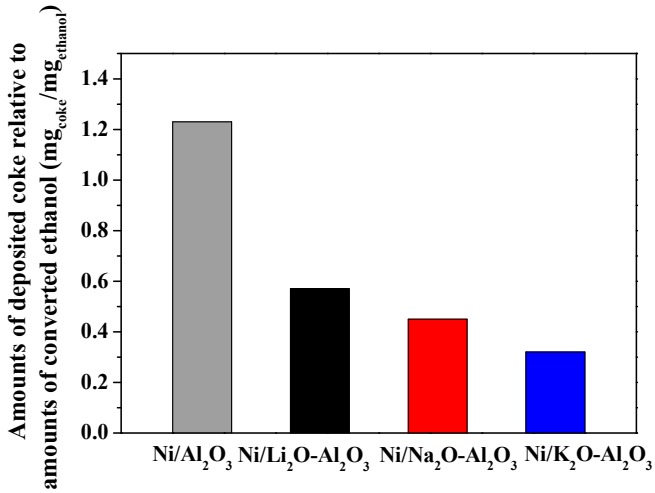


Figure 8. Coke analysis relative to converted ethanol.

Because alkali metals are known to provide basic sites for catalysts, basic sites in each catalysts were examined by CO_2-temperature programmed desorption (CO_2-TPD) (Figure 9) to elucidate the influence of basicity on coke deposition. The two main carbon dioxide desorption peaks appeared at 130 °C and 250–330 °C, which correspond to the

weak basic site and the strong basic site [31,35]. When alkali metals (Ni/M_2O-Al_2O_3) were added, the low temperature desorption peak was dominant for the alkali metal doped catalysts, while the high temperature desorption peak was dominant for Ni/Al_2O_3. The order of basic site quantity is as follows: Ni/K_2O-Al_2O_3 > Ni/Na_2O-Al_2O_3 > Ni/Li_2O-Al_2O_3 > Ni/Al_2O_3. This result shows that the alkali metals provide weak basic sites for nickel catalysts. In addition, the catalytic activity order is identical to the number of basic sites, except for Ni/Li_2O-Al_2O_3 (Figure 4). Considering that the low catalytic activity of Ni/L_2O-Al_2O_3 originated from the low surface area, we can infer that the increased catalytic activity of Ni/K_2O-Al_2O_3 and Ni/Na_2O-Al_2O_3 attributes to the basic sites. The correlation between number of basic sites and coke deposition is presented in Figure 10. The amounts of deposited coke decreased greatly on alkali metal promoted catalysts. This result shows that coke formation is inhibited by the weak basic sites that are offered by alkali metals.

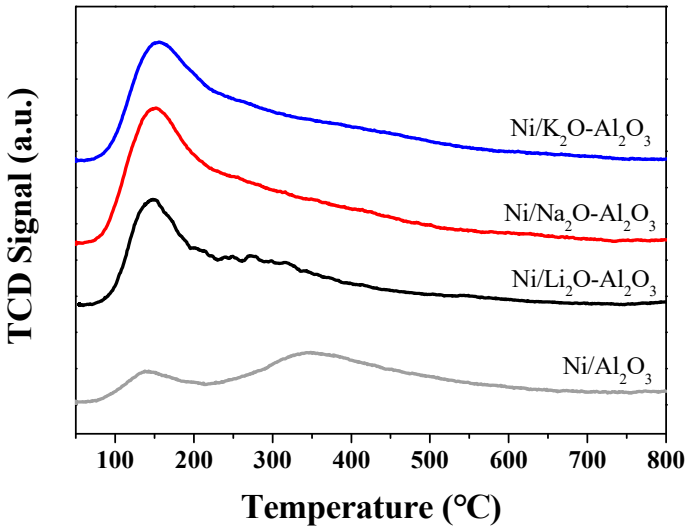


Figure 9. CO_2-TPD plots of Ni/M_2O-Al_2O_3.

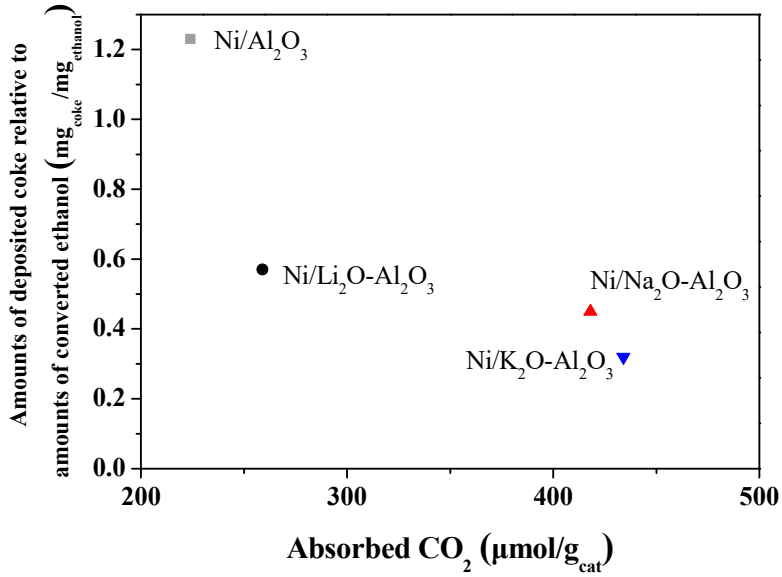


Figure 10. Amounts of deposited coke on Ni/M_2O-Al_2O_3 as a function of amounts of adsorbed carbon dioxide.

Analyses of spent catalysts and deposited coke suggest that the basic sites of nickel catalysts are critical to promote ethanol dry reforming and to reduce coke deposition.

Given that coke forms by unwanted reactions, i.e., ethanol dehydrogenation and ethanol dehydration (Figure 1 and Scheme 1), the direct reaction of ethanol and carbon dioxide should be accelerated to facilitate the formation of synthesis gas rather than methane and ethylene. This can be achieved by increasing the carbon dioxide concentration (Figure 2). In our catalytic system, the high carbon dioxide affinity of the basic sites induced by alkali metals plays a role similar to that of the high carbon dioxide concentration by increasing the local carbon dioxide concentration near the nickel active sites [36].

3. Materials and Methods

3.1. Catalyst Synthesis

Alkali metals were added to γ-Al_2O_3 (STREM, 97%, S_{BET} = 205 m^2/g) by incipient wetness impregnation. Calculated amounts of alkali metal precursor $LiNO_3$ (SAMCHUN, 99%), $NaNO_3$ (SAMCHUN, 99%), or KNO_3 (SHOWA, 99.5%) were dissolved into 4 mL of distilled water, and the resulting solution was added dropwise to 10 g of γ-Al_2O_3. The obtained solid was dried at 100 °C overnight, followed by calcination at 800 °C for 6 h which yielded M_2O-Al_2O_3 (M = Li, Na, or K, 5 wt%). The nickel catalysts were prepared by incipient wetness impregnation of $Ni(NO_3)_2{\cdot}6H_2O$ (Alfa Aesar) into the M_2O-Al_2O_3 support. The amount of nickel was adjusted to 10 wt%. The $Ni(NO_3)_2{\cdot}6H_2O$ aqueous solution (5.0 g $Ni(NO_3)_2{\cdot}6H_2O$ dissolved in 4.0 mL of distilled water) was added dropwise to 10 g of M_2O-Al_2O_3. Drying at 100 °C for 24 h and ensuing calcination at 800 °C for 6 h yielded Ni/M_2O-Al_2O_3 catalyst.

3.2. Catalyst Characterization

XRD analysis was implemented on a Rigaku Ultima IV with built-in a Cu K_α radiation (1.5418Å) to identify the crystal structures of the catalysts.

Nitrogen adsorption desorption isotherm analysis was performed using a Micromeritics Tristar II to clarify the pore characteristics of the catalysts. The surface area of the catalyst was calculated by the BET method and the pore structure was analyzed using the Barrett–Joyner–Halenda (BJH) model.

H_2-TPR was measured using a Micromeritics AutoChem II 2920. After filling the U-shaped quartz reactor with 0.15 g of catalyst, the pre-treatment process was carried out at 300 °C for 1 h under helium flow. Then, 10% H_2/Ar gas was flowed while increasing the temperature from 50 °C to 1000 °C at a ramp rate of 10 °C·min^{-1}.

CO_2-TPD was performed using a Micromeritics AutoChem II 2920. After filling the U-shaped quartz reactor with 0.13 g of catalyst, the pre-treatment process was carried out at 300 °C for 1 h under a helium flow, followed by reduction at 750 °C for 1 h using 5% H_2/Ar. Subsequently, helium gas was flowed to remove absorbed H_2 and 10% CO_2 was absorbed for 60 min at 50 °C. The carbon dioxide desorption was achieved by increasing the temperature from 100 °C to 900 °C at a ramp rate of 5 °C·min^{-1} under helium flow.

To confirm the amounts of deposited carbon, TGA was performed by TGA/DSC 1 STARe. The weight change was monitored by increasing the temperature from 25 °C to 930 °C at a ramp rate of 10 °C·min^{-1} in air. The amount of deposited carbon relative to amounts of reacted ethanol was calculated using the following Equation (3):

Amounts of deposited carbon relative to amounts of reacted ethanol =

$$\frac{\text{Amounts of carbon deposition for 10 h } \left(\frac{mg_{carbon}}{g_{catalyst}}\right)}{\text{Amounts of converted ethanol for 10 h } \left(\frac{mg_{ethanol}}{g_{catalyst}}\right)}. \quad (3)$$

Raman analysis was conducted to identify the type of carbon deposited on the catalysts using a Senterra (Bruker) device with a 532 nm laser at 20 mW. Transmission electron microscopy (TEM) images were obtained from a F200S (Talos) microscope operating at 200 kV.

3.3. Ethanol Dry Reforming

Figure 11 provides a schematic diagram of the ethanol dry reforming reactor system used in this study. A 1/2 inch quartz tube was used as a reactor and the temperature was controlled using a temperature controller inside the quartz tube. For ethanol dry reforming, 0.50 g of catalyst, shaped to have a diameter of 30–60 μm, was inserted and the temperature was increased to 750 °C under nitrogen flow. Then, the catalyst was reduced under flow of 5% H_2/He for 1 h at the same temperature. Ethanol dry reforming was conducted at 700 °C with a GHSV of 40,000 h^{-1}. The reaction gases were composed of 5 vol.% carbon dioxide and 5 vol.% ethanol balanced with helium for a carbon dioxide/ethanol ratio of 1, and 15 vol.% carbon dioxide and 5 vol.% of ethanol for carbon dioxide/ethanol ratio of 3. The product gases were analyzed by gas chromatography equipped with a thermal conductivity detector (Agilent Micro-GC 490, Molsieve 5A; H_2, CO, CH_4, Pora PLOT U; CO_2, C_2H_4, CP-Wax 52 CB; C_2H_5OH) and infrared spectrometer (Nicolet iS10, Thermo Fisher).

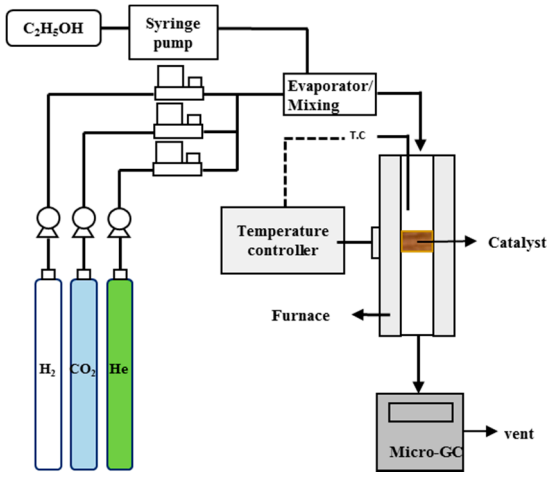


Figure 11. Schematic diagram of ethanol dry reforming reactor system.

Ethanol and carbon dioxide conversions were calculated using the following equation, Equation (4).

$$\text{Conversion } (\%) = \frac{\text{Carbon dioxide (or Ethanol)}_{\text{input}} - \text{Carbon dioxide (or Ethanol)}_{\text{output}}}{\text{Carbon dioxide (or Ethanol)}_{\text{input}}} \times 100 \quad (4)$$

4. Conclusions

The coke reduction effect of alkali metals on nickel catalyzed ethanol dry reforming was demonstrated. Moreover, the origin of catalyst deactivation was revealed to be coke deposition via ethanol dehydrogenation and dehydration. The alkali metals successfully inhibited coke formation and provided high catalytic activity and stability. To the best of our knowledge, this is the first report to employ alkali meals in ethanol dry reforming. The potassium modified nickel catalyst Ni/K_2O-Al_2O_3 showed the best performance among the investigated catalysts. TGA, Raman, and CO_2-TPD analyses verified that the high coke resistance of the alkali metal promoted catalysts attributed to the basic sites offered by alkali metals. The alkali metals reduced coke formation and accelerated coke removal rate by increasing the local carbon dioxide concentration near catalytic active sites. Following these results, the potassium could be utilized as a promoter for reducing coke formation in ethanol dry reforming.

Supplementary Materials: The following are available online at https://www.mdpi.com/2073-4344/11/2/260/s1, Figure S1: Plots of γ-Al_2O_3 catalyzed ethanol dry reforming performed at 700 °C, 40,000 h^{-1} GHSV, and ethanol/carbon dioxide ratio of 1. Figure S2: H_2-TPR plots Ni/M_2O-Al_2O_3, Figure S3: N_2-adsorption desorption isotherm plots of Ni/M_2O-Al_2O_3, Figure S4: BJH pore size distributions of (a) M_2O-Al_2O_3 and (b) Ni/M_2O-Al_2O_3, Figure S5: TEM images of reduced catalysts before ethanol dry reforming reaction. Figure S6: Time-dependent concentrations of methane and ethylene by ethanol dry reforming reaction, Figure S7: Plots of carbon dioxide and ethanol conversion by nickel catalysts at different temperatures of 550~700 °C, Figure S8: HAADF-STEM images and EDS analyses on spent catalysts after 10 h of ethanol dry reforming reaction.

Author Contributions: Conceptualization: J.H.L. and I.H.; Methodology: S.-W.P., Y.J.K., and J.H.P.; Investigation: S.-W.P., D.L., and S.-I.K.; Resources: I.H., T.S.C.; Writing—original draft: S.-W.P., D.L.; Writing—review and editing: Y.J.K., J.H.P., J.H.L., and T.S.C.; Supervision: J.H.L. and T.S.C. All authors have read and agreed to publish the manuscript.

Funding: This research was performed as project No. SI2111-20, funded by the Korea Research Institute of Chemical Technology (KRICT), and supported by the Technology Innovation Program (20012409, CO_2 upcycling cascade hydrogen production technology), funded by the Ministry of Trade, Industry & Energy (MOTIE, Korea), and supported by the National Research Council of Science & Technology (NST) grant by the Korea government (MSIP) No. CAP-16-05-KIMM.

Institutional Review Board Statement: Not applicable.

Informed Consent Statement: Not applicable.

Data Availability Statement: The data presented in this study are available on request from the corresponding author. The data are not publicly available due to privacy restrictions.

Conflicts of Interest: The authors declare no conflict of interest.

References

1. Grubb, M.; Vrolijk, C.; Brack, D. *Kyoto Protocol: A Guide and Assessment*, 1st ed.; Routledge: London, UK, 1999.
2. Climent, M.J.; Corma, A.; Iborra, S. Conversion of biomass platform molecules into fuel additives and liquid hydrocarbon fuels. *Green Chem.* **2014**, *16*, 516–547. [CrossRef]
3. Zhang, G.; Qu, J.; Su, A.; Zhang, Y.; Xu, Y. Towards understanding the carbon catalyzed CO_2 reforming of methane to syngas. *J. Ind. Eng. Chem.* **2015**, *21*, 311–317. [CrossRef]
4. Diaz, J.H. The influence of global warming on natural disasters and their public health outcomes. *Am. J. Disaster Med.* **2007**, *2*, 33–43. [CrossRef] [PubMed]
5. Gibbins, J.; Chalmers, H. Carbon capture and storage. *Energy Policy* **2008**, *36*, 4317–4322. [CrossRef]
6. Markewitz, P.; Kuckshinrichs, W.; Leitner, W.; Linssen, J.; Zapp, P.; Bongartz, R.; Schreiber, A.; Müller, T.E. Worldwide innovations in the development of carbon capture technologies and the utilization of CO_2. *Energy Environ. Sci.* **2012**, *5*, 7281–7305. [CrossRef]
7. Wang, J.; Cui, H.; Wei, S.; Zhuo, S.; Wang, L.; Li, Z.; Yi, W. Separation of biomass pyrolysis oil by supercritical CO_2 extraction. *Smart Grid Renew. Energy* **2010**, *1*, 98–107. [CrossRef]
8. Xu, W.; Liu, Z.; Johnston-Peck, A.C.; Senanayake, S.D.; Zhou, G.; Stacchiola, D.; Stach, E.A.; Rodriguez, J.A. Steam reforming of ethanol on Ni/CeO_2: Reaction pathway and interaction between Ni and the CeO_2 support. *ACS Catal.* **2013**, *3*, 975–984. [CrossRef]
9. Liu, C.-J.; Ye, J.; Jiang, J.; Pan, Y. Progresses in the preparation of coke resistant Ni-based catalyst for steam and CO_2 reforming of methane. *ChemCatChem* **2011**, *3*, 529–541. [CrossRef]
10. Wang, S.; Lu, G.Q.M. CO_2 reforming of methane on Ni catalysts: Effects of the support phase and preparation technique. *Appl. Catal. B* **1998**, *16*, 269–277. [CrossRef]
11. Hu, X.; Lu, G. Syngas production by CO_2 reforming of ethanol over Ni/Al_2O_3 catalyst. *Catal. Commun.* **2009**, *10*, 1633–1637. [CrossRef]
12. Du, X.; Zhang, D.; Shi, L.; Gao, R.; Zhang, J. Morphology dependence of catalytic properties of Ni/CeO_2 nanostructures for carbon dioxide reforming of methane. *J. Phys. Chem. C* **2012**, *116*, 10009–10016. [CrossRef]
13. Shi, Z. Nickel carbonyl: Toxicity and human health. *Sci. Total. Environ.* **1994**, *148*, 293–298. [CrossRef]
14. Bellido, J.D.A.; Tanabe, E.Y.; Assaf, E.M. Carbon dioxide reforming of ethanol over Ni/Y_2O_3–ZrO_2 catalysts. *Appl. Catal. B* **2009**, *90*, 485–488. [CrossRef]
15. Bahari, M.B.; Phuc, N.H.H.; Alenazey, F.; Vu, K.B.; Ainirazali, N.; Vo, D.-V.N. Catalytic performance of La-Ni/Al_2O_3 catalyst for CO_2 reforming of ethanol. *Catal. Today* **2017**, *291*, 67–75. [CrossRef]
16. Bahari, M.; Fayaz, F.; Ainirazali, N.; Huy, P.N.H.; Vo, D.-V.N. Evaluation of co-promoted Ni/Al_2O_3 catalyst for CO_2 reforming of ethanol. *J. Eng. Applied Sci.* **2016**, *11*, 7249–7253.

17. Cao, D.; Zeng, F.; Zhao, Z.; Cai, W.; Li, Y.; Yu, H.; Zhang, S.; Qu, F. Cu based catalysts for syngas production from ethanol dry reforming: Effect of oxide supports. *Fuel* **2018**, *219*, 406–416. [CrossRef]
18. Aziz, M.A.A.; Jalil, A.A.; Wongsakulphasatch, S.; Vo, D.-V.N. Understanding the role of surface basic sites of catalysts in CO_2 activation in dry reforming of methane: A short review. *Catal. Sci. Technol.* **2020**, *10*, 35–45. [CrossRef]
19. De Souza, G.; Balzaretti, N.; Marcilio, N.; Perez-Lopez, O. Decomposition of ethanol over Ni-Al catalysts: Effect of copper addition. *Procedia Eng.* **2012**, *42*, 335–345. [CrossRef]
20. Sivaramakrishnan, R.; Su, M.-C.; Michael, J.V.; Klippenstein, S.J.; Harding, L.B.; Ruscic, B. Rate constants for the thermal decomposition of ethanol and its bimolecular reactions with OH and D: Reflected shock tube and theoretical studies. *J. Phys. Chem. A* **2010**, *114*, 9425–9439. [CrossRef]
21. Xu, G.; Shi, K.; Gao, Y.; Xu, H.; Wei, Y. Studies of reforming natural gas with carbon dioxide to produce synthesis gas: X. The role of CeO_2 and MgO promoters. *J. Mol. Catal. A* **1999**, *147*, 47–54. [CrossRef]
22. Nederlof, C.; Talay, G.; Kapteijn, F.; Makkee, M. The role of RWGS in the dehydrogenation of ethylbenzene to styrene in CO_2. *Appl. Catal. A* **2012**, 59–68. [CrossRef]
23. Jabbour, K.; Massiani, P.; Davidson, A.; Casale, S.; El Hassan, N. Ordered mesoporous "one-pot" synthesized Ni-Mg(Ca)-Al_2O_3 as effective and remarkably stable catalysts for combined steam and dry reforming of methane (CSDRM). *Appl. Catal. B* **2017**, *201*, 527–542. [CrossRef]
24. Feng, B.; An, H.; Tan, E. Screening of CO_2 adsorbing materials for zero emission power generation systems. *Energy Fuels* **2007**, *21*, 426–434. [CrossRef]
25. Lu, H.; Reddy, E.P.; Smirniotis, P.G. Calcium oxide based sorbents for capture of carbon dioxide at high temperatures. *Ind. Eng. Chem. Res.* **2006**, *45*, 3944–3949. [CrossRef]
26. Wang, S.; Lu, G.Q. Effects of promoters on catalytic activity and carbon deposition of Ni/γ-Al_2O_3 catalysts in CO_2 reforming of CH_4. *J. Chem. Tech. Biotech.* **2000**, *75*, 589–595. [CrossRef]
27. Pegios, N.; Bliznuk, V.; Prünte, S.; Schneider, J.M.; Palkovits, R.; Simeonov, K. Comparative study on La-promoted Ni/γ-Al_2O_3 for methane dry reforming—Spray drying for enhanced nickel dispersion and strong metal—Support interactions. *RSC Adv.* **2018**, *8*, 606–618. [CrossRef]
28. Zangouei, M.; Moghaddam, A.Z.; Arasteh, M. The influence of nickel loading on reducibility of NiO/Al_2O_3 catalysts synthesized by sol-gel method. *Chem. Eng. Res. Bull.* **2010**, *14*, 97–102. [CrossRef]
29. Alberton, A.L.; Souza, M.M.; Schmal, M. Carbon formation and its influence on ethanol steam reforming over Ni/Al_2O_3 catalysts. *Catal. Today* **2007**, *123*, 257–264. [CrossRef]
30. Kim, P.; Joo, J.; Kim, H.; Kim, W.; Kim, Y.; Song, I.; Yi, J. Preparation of mesoporous Ni–alumina catalyst by one-step Sol–gel method: Control of textural properties and catalytic application to the hydrodechlorination of o-dichlorobenzene. *Catal. Lett.* **2005**, *104*, 181–189. [CrossRef]
31. Huang, L.Q.; Zhang, Z.H.; Guo, Z.L. The effect of MgO precoating on the perfomance of Ni/MgO-Al_2O_3 catalysts for carbon dioxide reforming of methane. *Adv. Mater. Res.* **2014**, *997*, 272–278. [CrossRef]
32. Chu, P.K.; Li, L. Characterization of amorphous and nanocrystalline carbon films. *Mater. Chem. Phys.* **2006**, *96*, 253–277. [CrossRef]
33. Marton, M.; Vojs, M.; Zdravecká, E.; Himmerlich, M.; Haensel, T.; Krischok, S.; Kotlar, M.; Michniak, P.; Vesely, M.; Redhammer, R. Raman spectroscopy of amorphous carbon prepared by pulsed arc discharge in various gas mixtures. *J. Spectrosc.* **2013**, *2013*, 1–6. [CrossRef]
34. Ferrari, A.C.; Robertson, J. Interpretation of Raman spectra of disordered and amorphous carbon. *Phys. Rev. B* **2000**, *61*, 14095–14107. [CrossRef]
35. Yu, C.; Ge, Q.; Xu, H.; Li, W. Effects of Ce addition on the Pt-Sn/γ-Al_2O_3 catalyst for propane dehydrogenation to propylene. *Appl. Catal. A* **2006**, *315*, 58–67. [CrossRef]
36. Álvarez, A.; Borges, M.; Corral-Pérez, J.J.; Olcina, J.G.; Hu, L.; Cornu, D.; Huang, R.; Stoian, D.; Urakawa, A. CO_2 Activation over catalytic surfaces. *Chem. Phys. Chem.* **2017**, *18*, 3135–3141. [CrossRef]